Agricultural and Forest Meteorology xxx (2010) xxx–xxx

Contents lists available at ScienceDirect

Agricultural and Forest Meteorology

journal homepage: www.elsevier.com/locate/agrformet

Assessing eddy-covariance flux tower location bias across the Fluxnet-Canada Research Network based on remote sensing and footprint modelling

Baozhang Chen[a,b,*], Nicholas C. Coops[b], Dongjie Fu[a], Hank A. Margolis[c], Brian D. Amiro[d], Alan G. Barr[e], T. Andrew Black[f], M. Altaf Arain[g], Charles P.-A. Bourque[h], Lawrence B. Flanagan[i], Peter M. Lafleur[j], J. Harry McCaughey[k], Steven C. Wofsy[l]

[a] *LREIS, Institute of Geographic Sciences & Nature Resources Research, Chinese Academy of Sciences, Beijing 100101, China*
[b] *Department of Forest Resource Management, 2424 Main Mall, University of British Columbia, Vancouver V6T 1Z4, Canada*
[c] *Faculté de foresterie, de géographie et de Géomatique, Université Laval, Québec G1K 7P4, Canada*
[d] *Department of Soil Science, University of Manitoba, Winnipeg, Manitoba R3T 2N2, Canada*
[e] *Climate Research Branch, Meteorological Service of Canada, Saskatoon, Saskatchewan S7N 3H5, Canada*
[f] *Faculty of Land and Food Systems, 2357 Main Mall, University of British Columbia, Vancouver V6T 1Z4, Canada*
[g] *School of Geography and Earth Sciences and McMaster Center For Climate Change, McMaster University, Hamilton, Ontario L8S 4K1, Canada*
[h] *Faculty of Forestry and Environmental Management, University of New Brunswick, Fredericton, New Brunswick E3B 6C2, Canada*
[i] *Department of Biological Sciences, University of Lethbridge, Lethbridge, Alberta T1K 3M4, Canada*
[j] *Department of Geography, Trent University, Peterborough, Ontario K9J 7B8, Canada*
[k] *Department of Geography, Queen's University, Kingston, Ontario K7L 3N6, Canada*
[l] *Department of Earth and Planetary Science, Harvard University, Cambridge, MA 02138, USA*

ARTICLE INFO

Article history:
Received 21 March 2010
Received in revised form
14 September 2010
Accepted 16 September 2010

Keywords:
SAFE footprint model
NDVI
EVI
Footprint climatology
Sensor location bias
Eddy covariance
Fluxnet
Carbon flux
Net ecosystem exchange

ABSTRACT

We describe an approach for evaluating the representativeness of eddy covariance flux measurements and assessing sensor location bias (SLB) based on footprint modelling and remote sensing. This approach was applied to the 12 main sites of the Fluxnet-Canada Research Network (FCRN)/Canadian Carbon Program (CCP) located along an east-west continental-scale transect, covering grassland, forest, and wetland biomes. For each site, monthly and annual footprint climatologies (i.e. monthly or annual cumulative footprints) were calculated using the Simple Analytical Footprint model on Eulerian coordinates (SAFE). The resulting footprint climatologies were then overlaid on to images of the Normalized Difference Vegetation Index (NDVI) and Enhanced Vegetation Index (EVI) derived from LANDSAT Thematic Mapper (TM) imagery, which were used as surrogates of land surface fluxes to estimate SLB. Results indicate that (i) the sizes of annual footprint climatology increased exponentially with increasing cumulative footprint percentages and, for a given percentage of footprint climatology, the footprint areas were significantly different among the sites. Typically, the 90% annual footprint climatology areas varied from 1.1 km^2 to 5.0 km^2; (ii) using either NDVI or EVI as the flux surrogate, the SLB was less than 5% for most sites with respect to the reference area of interest (A_r) at 90% annual footprint climatology (scenario A) and a circular area with radius of 1 km centred at the individual tower (scenario B), with several exceptions; (iii) the SLB decreased with increasing size of footprint climatology for all sites for both scenarios A and B; (iv) out of 12, eight flux towers represented most of the ecosystem surrounding the towers for an area of 0.3 km^2 up to 10 km^2 with a satisfactorily low bias of <5%, whereas four towers represented areas ranging from only 0.75 to 4 km^2; and (v) the seasonal differences in monthly SLB using NDVI as a flux surrogate were about 1–4% for most sites for both scenarios A and B.

* Corresponding author at: Department of Forest Resource Management, 2424 Main Mall, University of British Columbia, Vancouver V6T 1Z4, Canada. Tel.: +1 604 822 6592, fax: +1 604 822 9106.
E-mail addresses: baozhang.chen0808@gmail.com (B. Chen), nicholas.coops@ubc.ca (N.C. Coops), fudongjie@gmail.com (D. Fu), Hank.Margolis@sbf.ulaval.ca (H.A. Margolis), brian_amiro@umanitoba.ca (B.D. Amiro), alan.barr@ec.gc.ca (A.G. Barr), andrew.black@ubc.ca (T.A. Black), arainm@mcmaster.ca (M.A. Arain), cbourque@unb.ca (C.P.-A. Bourque), larry.flanagan@uleth.ca (L.B. Flanagan), plafleur@trentu.ca (P.M. Lafleur), mccaughe@queensu.ca (J.H. McCaughey), scw@io.harvard.edu (S.C. Wofsy).

0168-1923/$ – see front matter © 2010 Elsevier B.V. All rights reserved.
doi:10.1016/j.agrformet.2010.09.005

1. Introduction

The eddy covariance (EC) technique, based on measurements of turbulent fluctuations of the vertical wind velocity and the concentration variations of a passive tracer, is a commonly applied method to measure directly the exchanges of energy, water and carbon between vegetation and the atmosphere. The number of EC flux towers has been rapidly increasing (Baldocchi, 2008), and today, there exist more than 500 EC-flux towers globally. Turbulent flux measurements provide information on the gas exchange between vegetation and the atmosphere which are characteristic for a given ecosystem of interest (Schmid and Lloyd, 1999). Networks of EC systems have been set up at local to continental scales based loosely on the idea that individual nodes are representative of a large area (Baldocchi, 2008; Chasmer et al., 2008). However, utilisation and application of EC measurements (especially for spatial up-scaling of these measurements to landscape and regional scales) can be problematic due to difficulties/uncertainties in assessing/interpreting the associated measuring biases of EC data arising from the sensor's views over heterogeneous natural vegetation from different wind sectors (Schmid, 1997, 2002; Soegaard et al., 2003; Gockede et al., 2004; Rebmann et al., 2005; Chen et al., 2009a). The adoption of the EC technique to estimate surface exchange is based on the assumption that the contributing area of the fluxes is topographically flat and the vegetation extends uniformly within the footprint area (Foken and Wichura, 1996; Baldocchi, 2003, 2008; Finnigan et al., 2003). In reality however, natural vegetation is spatially heterogeneous (Chen et al., 2007; Baldocchi, 2008) causing the EC method to be vulnerable to bias errors under non-ideal conditions, for instance if the EC tower is located in a complex landscape (Goulden et al., 1996; Finnigan et al., 2003). There is a potential bias in observations associated with tower location relative to land-surface heterogeneities, and these are comparatively less well assessed than the other major potential sources of error such as random errors related to the atmospheric turbulence conditions and the underlying vegetation (Richardson et al., 2006) and systematic bias errors associated with different sensor configurations and turbulence-data processing (Baldocchi, 2008).

The interpretation of EC flux measurements over a heterogeneous surface depends largely on the estimation of the flux footprint probability distribution function (PDF). The dimensions and orientation of the turbulent flux footprint are dependent on the height of the measurement, the surface roughness length, lateral turbulence, wind speed, wind direction, and atmospheric stability (Schmid, 1994). Although many advances have been made in footprint modelling and experimental validation (e.g. Leclerc and Thurtell, 1990; Wilson and Swaters, 1991; Horst and Weil, 1994; Finn et al., 1996; Kormann and Meixner, 2001; Leclerc et al., 2003), the influence of the variability of footprint and vegetation heterogeneities on EC flux measurements has not yet been investigated fully.

It has also been recognised that footprint climatologies (e.g. seasonal, annual and multi-year footprint PDF) provide crucial information about the vegetation being sampled when measuring seasonal and annual fluxes (e.g. Amiro, 1998; Schmid and Lloyd, 1999; Stoughton et al., 2000). One of the practical problems when applying footprint modelling to examine the representativeness of an EC flux tower is that the source strength distribution over the footprint area is unknown *a priori* (Schmid and Lloyd, 1999; Kim et al., 2006). Thus, it is required to estimate the spatial distribution of the surface source strength, which is usually determined by the vegetation characteristics and soil conditions. Satellite-borne remote sensing provides moderate-spatial resolution images (30–100 m) of the land surface and has successfully been used for a number of decades to parameterize vegetation characteristics over large spatial extents at variable time intervals (e.g. Moran et al., 1997; Running et al., 2004). Studies on the use of satellite-derived vegetation reflectance indices have shown that these indices are significantly correlated with carbon or water flux strength (Moran and Jackson, 1991; Moran et al., 1994, 1995, 1996; Nouvellon et al., 2001; Holifield et al., 2003; Bergheime et al., 2006), and as a result remotely sensed vegetation indices can provide a surrogate of the surface flux source strength. Therefore, the combination of footprint climatology modelling and remotely sensed moderate-resolution image data can potentially be used to assess the representativeness, more formally the sensor location bias (SLB), of an EC flux tower over a heterogeneous surface area (Kim et al., 2006; Chen et al., 2009a).

The objective of this study is to assess the SLB across the Fluxnet Canada Research Network (FCRN)/Canadian Carbon Program (CCP). The footprint climatologies at multi-temporal scales (i.e. monthly and annual) were calculated using the Simple Analytical Footprint model on Eulerian coordinates (SAFE, Chen et al., 2008, 2009a). The Normalized Difference Vegetation Index (NDVI) and the Enhanced Vegetation Index (EVI), derived from LANDSAT Thematic Mapper (TM) or Enhanced Thematic Mapper (ETM+) data, were used as surrogates of land surface fluxes. The flux footprint climatology maps were then superimposed on the vegetation indices for the 12 individual FCRN towers, and finally, the SLB for each site was assessed.

2. Site characteristics, tower measured data and LANDSAT images

In this study, we selected 12 FCRN/CCP sites covering four broad biome types (grassland, wetland, and both temperate and boreal forests), which are distributed along an east-west continental-scale transect in the southern portion of Canada (Fig. 1). Site and EC flux tower characteristics are summarised in Tables 1 and 2 (http://www.fluxnet-canada.ca).

Year-round half-hourly flux and meteorological measurements made in 2006, which was generally considered a normal weather year over most of the sites, were used in this study. These data include wind direction (WD), wind speed (u), standard deviation of lateral wind speed (σ_v), friction velocity (u_*) and sensible and latent heat fluxes. Missing flux and meteorological data were filled using the gap-filling method of Chen et al. (2009b). Those gap-filled datasets were used to drive the footprint model for assessing monthly and annual footprint climatology for all the sites.

LANDSAT imagery acquired in 2006, or as close as possible, was acquired at each of the 12 sites with a 6 km × 6 km area centered on the tower locations downloaded from the U.S. Geological Survey at http://glovis.usgs.gov/. The scene path and row and the acquisition dates are shown in Table 3. The false color composite images (bands 2, 3 and 4) for each domain (6 km × 6 km) centred at individual towers are shown in Fig. 2 with land-surface heterogeneities apparent across and within sites. The 90% contour of cumulative annual footprint climatology FDP and a circle with 1-km radius centred at each tower are also shown.

3. Theory and methodology

3.1. Point-to-area representativeness

Nappo et al. (1982) defined representativeness as "the extent to which a set of measurements taken in a given space-time domain reflects the actual conditions in the same or different space-time domain taken on a scale appropriate for a specific application." In this study, we are primarily interested in the "point-to-area representativeness", which describes the extent to which a set of measurements made at a point reflects the actual aggregated conditions in the same time domain but over an appropriately extended spatial domain (i.e. an ecosystem of interest or a flux footprint area).

Please cite this article in press as: Chen, B., et al., Assessing eddy-covariance flux tower location bias across the Fluxnet-Canada Research Network based on remote sensing and footprint modelling. Agric. Forest Meteorol. (2010), doi:10.1016/j.agrformet.2010.09.005

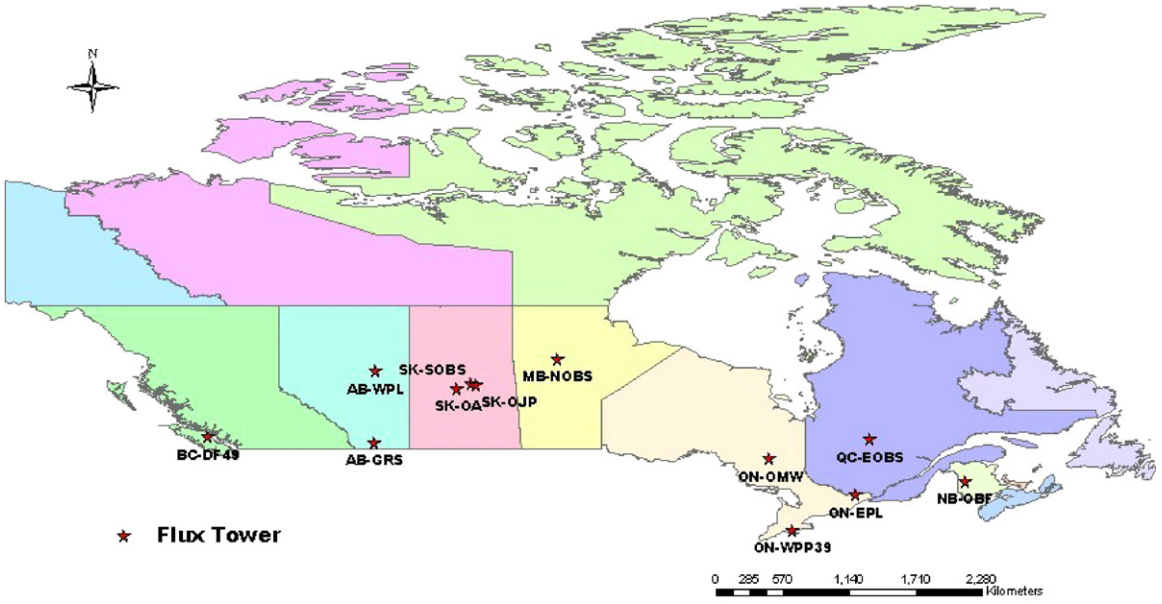

Fig. 1. Locations of flux towers in the Fluxnet Canada Research Network/Canadian Carbon Program (CCP). For description of flux sites, see Tables 1 and 2.

To evaluate whether a point-to-area representativeness in a specific case is satisfied or not, we first set up an assessment criterion. Following Nappo et al. (1982), a criterion (δ) is defined as,

$$Pr\left\{\frac{(\gamma-\bar{\gamma})^2}{\bar{\gamma}^2}\le\delta^2\right\}=\Gamma, \quad (1)$$

where Γ is the probability that the difference between a quantity γ, measured at a reference location (e.g. flux tower) and the area-averaged value $\bar{\gamma}$ over an appropriate spatial domain (e.g. an ecosystem of interest or a flux footprint area), lies within $\pm\delta$. Schmid and Lloyd (1999) defined the sensor (tower) location bias

Table 1
List of abbreviations, key attributes of vegetation at FCRN sites.

Abbreviation of vegetation type[a]	Site[b]	Vegetation type	Overstory	Understory and groundcover	References
CBF	MB-NOBS	Coniferous boreal forest	*Picea mariana*	*Bryophytes*	Dunn et al. (2007) and Turner et al. (2003)
	QC-EOBS	Coniferous boreal forest	*Picea mariana*, *Pinus banksiana*	*Ericaceae*, *bryophytes*	Richardson et al. (2006)
	SK-OJP	Coniferous boreal forest	*Pinus banksiana*	*Alnus crispa*, *lichens*	Barr et al. (2006)
	SK-SOBS	Coniferous boreal forest	*Picea mariana*	*Bryophytes*	Barr et al. (2006)
CMF	NB-OBF	Coniferous maritime forest	*Abies balsamea*	*Cornus canadensis*, *bryophytes*, *pteridophytes*	Xing et al. (2007)
CTF	BC-DF49	Coniferous temperate rainforest	*Pseudotsuga menziesii*	*Achlys triphylla*, *Berberis aquifolium*, *bryophytes*	Chen et al. (2009b)
	ON-WPP39	Coniferous temperate forest	*Pinus strobus*	*Prunus serotina*, *Quercus alba*, *Q. velutina*, *Abies balsamea*, *Rhus radicans*, *pteridophytes*, *bryophytes*	Arain and Restrepo-Coupe (2005) and Peichl et al. (2010)
DBF	SK-OA	Deciduous boreal forest	*Populus tremuloides*	*Corylus cornuta*	Barr et al. (2006)
GRL	AB-GRS	Short/mixed grass prairie (C3); grassland	–	*Agropyron dasystachyum*, *A. smithii*	Flanagan and Johnson (2005), Flanagan et al. (2002) and Richardson et al. (2006)
MBF	ON-OMW	Mixedwood boreal forest	*Populus tremuloides*, *Picea mariana*, *Picea glauca*, *Betula papyrifera*, *Abies balsamea*	*Cornus canadensis*, *bryophytes*, *pteridophytes*	McCaughey et al. (2006)
WL	AB-WPL	Treed fen; wetland	*Larix laricina*, *Picea mariana*	*Betula pumila*, *Ledum groenlandicum*, *Salix spp.*, *bryophytes*	Flanagan (2009) and Syed et al. (2006)
	ON-EPL	Ombrotrophic bog; wetland	–	Ledum groenlandicum, *Chamaedaphne calyculata*, *Kalmia augustifolium*, *Vaccinium myrtilloides*, *bryophytes*	Admiral and Lafleur (2007) and Peichl et al. (2010)

[a] Vegetation types: CBF, coniferous boreal forest; CMF, coniferous maritime forest; CTF, coniferous temperate forest; DBF, deciduous boreal forest; GRL, Grassland; MBF, mixed wood boreal forest; WL, Wetland.
[b] Site names: First two letters indicate the province (MB, Manitoba; QC, Quebec; SK, Saskatchewan; NB, New Brunswick; BC, British Columbia; ON, Ontario; AB, Alberta); NOBS, Northern Old Black Spruce; EOBS, Eastern Old Black Spruce; OJP, Old Jack Pine; SOBS, Southern Old Black Spruce; OBF, Old Balsam Fir; DF49, Douglas fir (established 1949); WPP39, White Pine Plantation (established 1939); OA, Old Aspen; GRS, grassland; OMW, Old mixedwood; WPL, Western peatland; EPL, Eastern peat land).

Please cite this article in press as: Chen, B., et al., Assessing eddy-covariance flux tower location bias across the Fluxnet-Canada Research Network based on remote sensing and footprint modelling. Agric. Forest Meteorol. (2010), doi:10.1016/j.agrformet.2010.09.005

Table 2
List of abbreviations, site characteristics and tower measurement information for FCRN sites.[a]

Vegetation type[b]	Site[b]	LAI ($m^2\ m^{-2}$)	T_e (year)	h_m (m)	h_c (m)	u_*^{th} ($m\ s^{-1}$)	u ($m\ s^{-1}$)	Latitude (°N)	Longitude (°W)	H_e (m)	References
CBF	MB-NOBS	4.1	1845	29	9.1	0.25	3.3	55.87956	98.48084	259	Dunn et al. (2007) and Turner et al. (2003)
	QC-EOBS	3.7	1898	24	13.8	0.25	2.6	49.69247	74.34204	387	Richardson et al. (2006)
	SK-OJP	3.4	1929	29	13.7	0.35	3.0	53.91634	104.69203	579	Barr et al. (2006)
	SK-SOBS	5.6	1879	25	13.7	0.35	3.3	53.98717	105.11779	629	Barr et al. (2006)
CMF	NB-OBF	8.4	1967	18.5	14	0.40	2.9	46.47388	67.09937	341	Xing et al. (2007)
CTF	BC-DF49	6.1	1949	43	33	0.30	1.8	49.86883	125.33508	320	Chen et al. (2009b)
	ON-WPP39	8.0	1939	28	21.8	0.35	2.4	42.71222	80.3572	184	Arain and Restrepo-Coupe (2005) and Peichl et al. (2010)
DBF	SK-OA	3.8	1919	39	21	0.35	3.2	53.62889	106.19779	601	Barr et al. (2006)
GRL	AB-GRS	0.88	–	6	0.365	0.25	4.6	49.70919	112.94025	951	Flanagan and Johnson (2005), Flanagan et al. (2002), Flanagan (2009) and Richardson et al. (2006)
MBF	ON-OMW	3.0	1930	43.3	31.0	0.30	3.6	48.21738	82.15553	341	McCaughey et al. (2006)
WL	AB-WPL	2.6	1958[c]	9	Tree:3	0.15	2.0	54.95384	112.46698	626	Syed et al. (2006)
	ON-EPL	1.4	–	3.0	Shrub:0.25	0.10	2.3	45.40940	75.51870	70	Admiral and Lafleur (2007) and Peichl et al. (2010)

[a] LAI, T_e, h_m, h_c, u_*^{th}, u and H_e are leaf area index, established time, EC sensor height, canopy height, friction wind speed (u_*) threshold for EC flux calculation, annual mean wind speed and elevation above sea level, respectively. Values of h_m, h_c, u_*^{th} and u are for 2006.

[b] See Table 1 for description of abbreviation of vegetation type and site name.

[c] 1958 for *Larix laricina* and 1870 for *Picea mariana*.

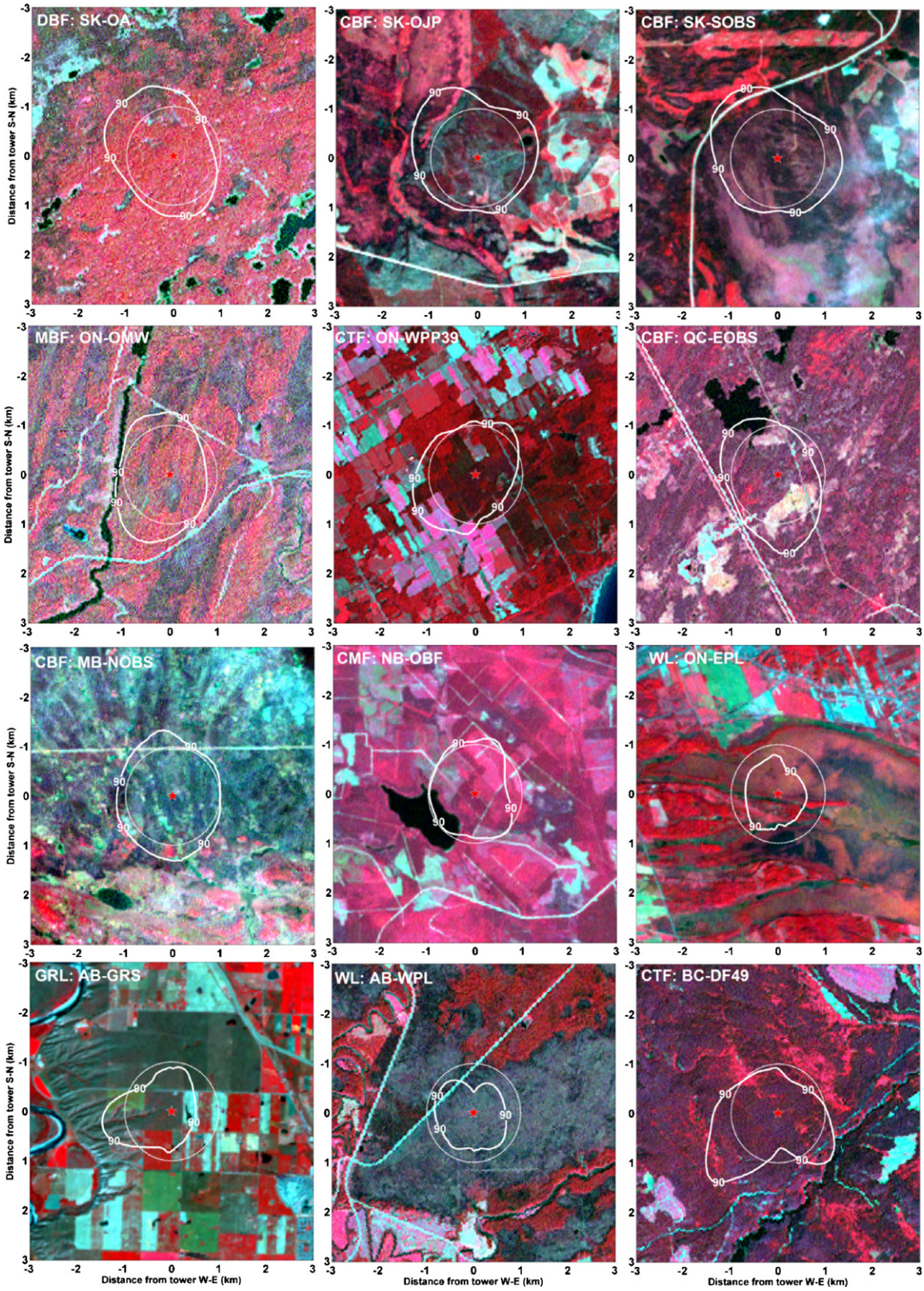

Fig. 2. False color composite images (bands 2, 3 and 4) of LANDSAT at a 30-m resolution for each area (6 km × 6 km) centred at individual FCRN towers. The scene path and row and the acquired dates are shown in Table 3. The 90% contour of cumulative annual footprint climatology PDF and a circle with 1-km radius centred at the tower overlie their corresponding LANDSAT imagery maps. For description of abbreviation of vegetation type and site name, see Table 1.

Please cite this article in press as: Chen, B., et al., Assessing eddy-covariance flux tower location bias across the Fluxnet-Canada Research Network based on remote sensing and footprint modelling. Agric. Forest Meteorol. (2010), doi:10.1016/j.agrformet.2010.09.005

Table 3
Acquired LANDSAT imagery information for FCRN sites used in this study.

Vegetation type[a]	Site ID [a]	Satellite	Dataset	Path	Row	Acquired date
CBF	MB-NOBS	LANDSAT7	ETM+	034	021	2006/09/06
	QC-EOBS	LANDSAT4-5	TM	016	025	2002/08/28
	SK-OJP	LANDSAT7	ETM+	037	022	2006/08/26
	SK-SOBS	LANDSAT7	ETM+	037	022	2006/08/26
CMF	NB-OBF	LANDSAT7	ETM+	010	028	2005/08/26
CTF	BC-DF49	LANDSAT4-5	TM	049	025	2000/06/26
	ON-WPP39	LANDSAT4-5	TM	018	030	1999/09/03
DBF	SK-OA	LANDSAT4-5	TM	038	023	2001/08/03
GRL	AB-GRS	LANDSAT7	ETM+	041	025	2006/07/21
MBF	ON-OMW	LANDSAT4-5	TM	020	027	2002/09/09
WL	AB-WPL	LANDSAT4-5	TM	042	022	2001/08/15
	ON-EPL	LANDSAT7	ETM+	015	029	2005/09/14

[a] See Table 1 for description of abbreviation of vegetation type and site name.

(Δ) based on Eq. (1) as,

$$\Delta = \frac{(\gamma - \bar{\gamma})}{\bar{\gamma}^2}. \quad (2)$$

In this application, γ corresponds to the carbon or water fluxes measured on the EC tower, while $\bar{\gamma}$ is the spatially averaged respective fluxes over an area of interest. If the actual distribution of surface flux source strength $\gamma_i(x,y)$ and footprint PDF $\phi(x,y)$ are known, γ can be estimated following Chen et al. (2009a) as,

$$\gamma = \iint_{\Omega_\Pi} \gamma_i(x,y)\phi(x,y)dxdy, \quad (3)$$

where Ω_Π is the footprint source area within the cumulative footprint percentage Π, and Π could be any value between 1% and 99%. $\bar{\gamma}$ can be considered as an un-weighted average of $\gamma_i(x,y)$ over a land surface of interest.

3.2. Footprint and footprint climatology modelling

3.2.1. Footprint PDF modelling

In this study we use the Simple Analytical Footprint model on Eulerian coordinates (SAFE, Chen et al., 2009a) to compute the footprint PDF. The SAFE model is developed on the basis of the two-dimensional Eulerian advection–diffusion equation (Horst and Weil, 1992) and its analytical solution relies on a sophisticated formulation of van Ulden (1978) using parameterization methods in Gryning et al. (1987), Finn et al. (1996) and Kormann and Meixner (2001). This analytical solution takes into account atmospheric stability and uses the wind velocity power law above the canopy, allowing it to be applicable to all conditions of atmospheric stability. In SAFE, the flux footprint PDF, $f(x,y,z_m)$ in m^{-2}, is defined as the product of the crosswind concentration distribution function $D_y(x,y)$ in m^{-1} and the crosswind-integrated footprint, $f^y(x,z_m)$ in m^{-1} (Pasquill and Smith, 1983; van Ulden, 1978; Horst and Weil, 1992). The SAFE model input includes the EC sensor height (h_m), canopy height (h_c), roughness length (z_0), friction wind speed threshold for EC flux calculation (u_*^{th}), and several meteorological variables (WD, u, σ_v and u_*) and sensible and latent heat fluxes measured at the EC sensor height. Values of h_m, h_c, u_*^{th} are taken from the literature as shown in Table 2 and z_0 is approximated as 10% of h_c. The detailed description of the footprint model can been found in Chen et al. (2009a).

In this study, the model was run at half-hourly time steps at a pixel (grid) size of 30 m × 30 m (consistent with the LANDSAT spatial resolution) covering the area (6 km × 6 km) centred on the tower.

3.2.2. Footprint climatology PDF modelling

The half-hourly footprint PDFs were rotated along the wind direction and then accumulated to yield monthly, seasonal or annual values of the footprint climatology PDF, $\phi(x,y,z_m)$. During nighttime, the half-hourly footprints were only computed when $u_* > u_*^{th}$ (u_*^{th} values for each site are shown in Table 2). The accumulated footprint PDF was normalized by the interested cumulative footprint (Π) area (Ω_Π) to yield the footprint climatology PDF (ϕ) for each pixel as,

$$\phi(x,y,z_m) = \frac{\sum_{i=1}^{N} f(x,y,z_m)}{\iint_{\Omega_\Pi} \sum_{i=1}^{N} f(x,y,z_m)dxdy}, \quad (4)$$

where i is the time step (i.e., 30 min) and N is the total number of 30-min periods within the timeframe (i.e., month, season, or year). In the model implementation, we sorted $f(x,y,z_m)$ values in descending order and then accumulated the values from the largest to the smallest until a given fraction Π is achieved. The source area Ω_Π includes all grids (cells) that have $f(x,y,z_m)$ larger than the cut-off point, and the fraction Π is the ratio of the cumulative footprint function within Ω_Π to the whole integrated source function,

$$\Pi = \frac{\varphi_\Pi}{\varphi_{tot}} = \frac{\iint_{\Omega_\Pi} f(x,y,z_m)dxdy}{\int_{-\infty}^{\infty}\int_{-\infty}^{\infty} f(x,y,z_m)dxdy}, \quad (5)$$

where φ_Π and φ_{tot} are the integrals of the footprint function over Ω_Π and the total area, respectively. In this study, we set Π to be 0.99. The model domain should be large enough to cover the interested cumulative footprint Π area, Ω_Π. The total weighted footprint $\Phi = \iint_{\Omega_\Pi} \phi(x,y,z_m)dxdy$ within the model domain was normalized to equal to 1.

3.3. Analysis of LANDSAT images

The LANDSAT imagery was georeferenced and atmospherically corrected using the cosine approximation model (COST) of Wu et al. (2005) and radiometrically normalized following the method of Hall et al. (1991). NDVI and EVI were then derived to describe the land surface heterogeneity as a surrogate of surface flux as these different vegetation indices reflect somewhat different vegetation characteristics.

3.3.1. Normalized Difference Vegetation Index (NDVI)

NDVI (Tucker, 1979; Field et al., 1995) is calculated as,

$$\text{NDVI} = \frac{\rho_{nir} - \rho_{red}}{\rho_{nir} + \rho_{red}}, \quad (6)$$

where ρ_{nir} and ρ_{red} are the reflectance in the near infrared and red bands, respectively. NDVI is generally related to green vegetation cover or vegetation canopy density and has been shown to be well

Please cite this article in press as: Chen, B., et al., Assessing eddy-covariance flux tower location bias across the Fluxnet-Canada Research Network based on remote sensing and footprint modelling. Agric. Forest Meteorol. (2010), doi:10.1016/j.agrformet.2010.09.005

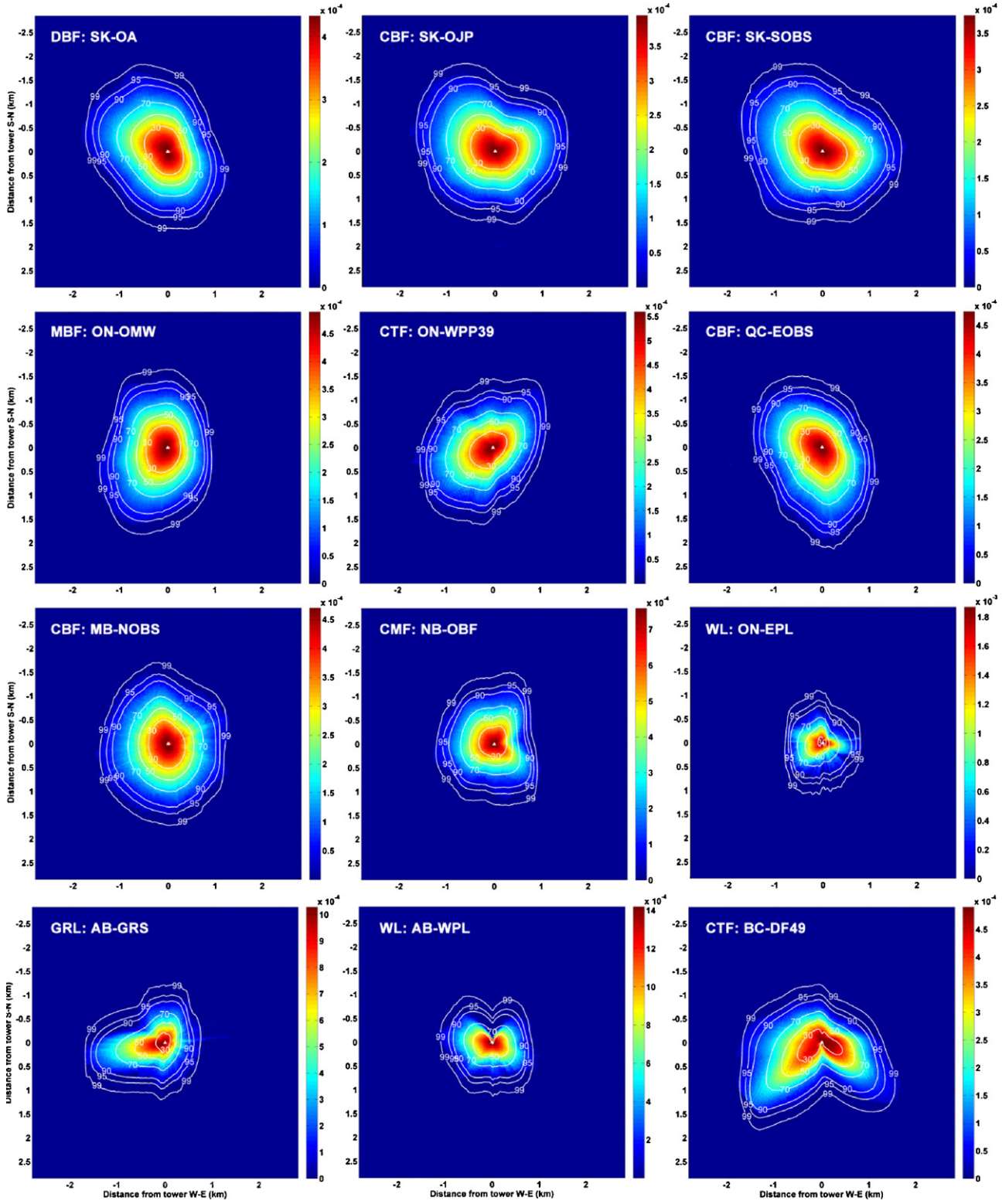

Fig. 3. Annual footprint climatology PDF maps in 2006 for the 12 FCRN sites. The cumulative footprint contours overlie their corresponding footprint PDF maps. For description of abbreviation of vegetation type and site name, see Table 1.

Please cite this article in press as: Chen, B., et al., Assessing eddy-covariance flux tower location bias across the Fluxnet-Canada Research Network based on remote sensing and footprint modelling. Agric. Forest Meteorol. (2010), doi:10.1016/j.agrformet.2010.09.005

correlated with green leaf area index (LAI) and biomass (e.g., Sellers, 1985; Govind et al., 2009).

3.3.2. Enhanced Vegetation Index (EVI)

EVI is similar to NDVI but uses spectral information from the blue band (ρ_{blue}). Following Huete et al. (1997) it is computed,

$$\mathrm{EVI} = \frac{G \times (\rho_{nir} - \rho_{red})}{(\rho_{nir} + C_1 \times \rho_{red} - C_2 \times \rho_{blue} + L)}, \quad (7)$$

where $G = 2.5$, $C_1 = 6$, $C_2 = 7.5$, and $L = 1$. EVI is found to be significantly correlated with the fraction of the photosynthetically active radiation absorbed by leaf chlorophyll in the canopy providing a good surrogate of the spatial variability index for photosynthesis rate (e.g. Xiao et al., 2004).

3.3.3. Sensor location bias (SLB)

The SLB, Δ after Schmid and Lloyd (1999), was computed using Eq. (2). Kim et al. (2006) and Chen et al. (2009a) also used root bias ($\sqrt{\Delta}$) to quantify the spatial representativeness of a footprint. It is important to note that Δ does not indicate the direction of the bias (over- or under-estimation). In this study, analogous to the concept proposed by Schmid and Lloyd (1999), SLB is expressed as the difference between the weighted surface source strengths by the flux footprint PDF and the un-weighted (simply-aggregated) surface source strengths for the reference area of interest (A_r), standardised by the un-weighted surface source strengths. A notation of δ is used for SLB, which preserves the sign information with positive or negative symbols indicating overestimated bias or underestimated bias, respectively. If we approximate the vegetation index λ (=NDVI or EVI) as a surrogate of the land surface source strength (e.g. C flux), δ can be calculated as,

$$\delta = \frac{\lambda_\phi - \bar{\lambda}}{\bar{\lambda}}, \quad (8)$$

where λ_ϕ and $\bar{\lambda}$ are the footprint-PDF-weighted vegetation index λ (=NDVI or EVI) and the un-weighted (simply averaged) λ over an area of interest, respectively. The footprint-PDF-weighted λ_ϕ is calculated using a discrete adaptation of Eq. (3),

$$\lambda_\phi = \sum_{i=1}^{N_\Pi} \lambda_i \phi_i, \quad (9)$$

where N_Π is the total number of pixels in the footprint climatology area within the given cumulative footprint-climatology percentage (Π) ranging from 1% to 99%. The un-weighted vegetation index $\bar{\lambda}$ is computed as,

$$\bar{\lambda} = \frac{1}{N} \sum_{i=1}^{N} \lambda_i, \quad (10)$$

where N is the total number of pixels in the reference area (A_r) of interest for the ecosystem (e.g. a regular circular area centred at the tower or an area of an ecosystem delimited with clear boundaries or one fixed satellite image pixel).

In this study, monthly and annual SLB (δ) using NDVI and EVI as flux surrogates were computed for the 12 sites with the cumulative footprint-climatology percentage (Π) varying from 1 to 99% for Eqs. (9) and (10) in four scenarios: (i) in scenario A, A_r is assumed to be 90% of annual footprint climatology area (A_{90}), and (ii) in scenarios B, C, and D, A_r is assumed to be circular areas centred at the individual towers with radii (r) of 1 km, 2 km and 3 km, respectively.

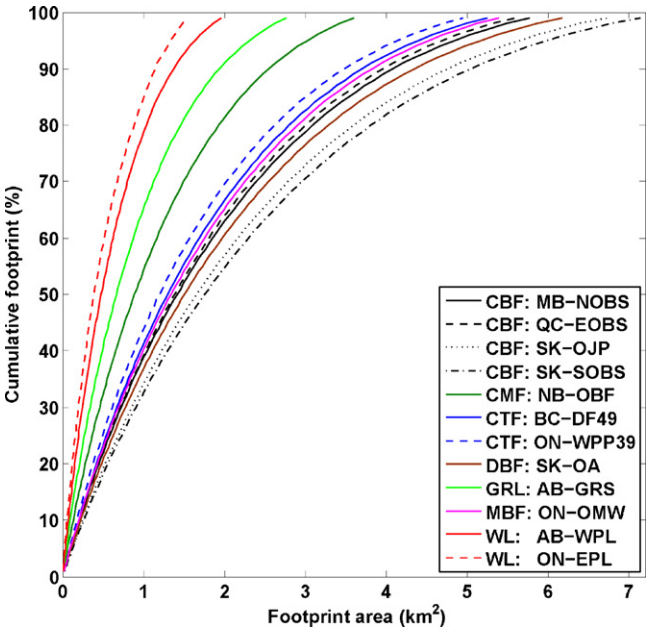

Fig. 4. Exponential relationship between the annual cumulative footprint climatology percentages and their corresponding areas for the 12 FCRN sites. For description of abbreviation of vegetation type and site name, see Table 1.

4. Results

4.1. Footprint climatology

Fig. 3 shows the distributions of the 2006 annual footprint-climatology PDFs, as well as the derived cumulative footprint contours at each site. For most sites, the annual footprint PDF is distributed asymmetrically around the tower. The relationship between the annual cumulative footprint-climatology percentages and its corresponding area for each site is shown in Fig. 4 and Table 4. The areas of annual footprint-climatology exponentially increased with increasing cumulative footprint-climatologies for all sites, however, the sizes and orientations of annual footprint climatology differed among the 12 sites. For example, the annual footprint sizes of wetlands (AB-WPL and ON-EPL) and prairie (AB-GRS) were much smaller than those of forest sites (Figs. 3 and 4 and Table 4). The sizes of the 90% annual cumulative footprint climatologies varied from 1.14 km^2 (ON-EPL) to 5.04 km^2 (SK-SOBS). By assuming the footprint is circular centred at the individual towers, the corresponding mean "radius" (r) of footprint was calculated as $r_\Pi = \sqrt{\frac{A_\Pi}{\pi}}$, where A_Π is the footprint area for a given Π cumulative percentage. The values of r_{80}, r_{90} and r_{99} are shown in Table 4. Four of the 12 sites had a r_{90} value less than 1 km: the wetland sites (AB-WPL and ON-EPL), the prairie site (AB-GRS) and the coniferous maritime forest site (NB-OBF).

Most of the FCRN sites experienced large seasonal variations in the size of footprint climatology (Fig. 5). The seasonal differences in the size of 90% monthly footprint climatology varied from 0.69 km^2 (ON-EPL) to 2.48 km^2 (SK-SOBS). The patterns and orientations of footprint climatology varied month to month for most sites, consistent with seasonal changes in prevailing wind directions, wind speed and vegetation heights at the prairie and wetland sites.

4.2. Sensor location bias

To assess potential differences in EC tower measured fluxes and the expected spatial aggregate of the surface exchanges for the ecosystem of interest, the annual and monthly footprint PDFs were compared to the NDVI and EVI images for individual sites and the

Please cite this article in press as: Chen, B., et al., Assessing eddy-covariance flux tower location bias across the Fluxnet-Canada Research Network based on remote sensing and footprint modelling. Agric. Forest Meteorol. (2010), doi:10.1016/j.agrformet.2010.09.005

Table 4
Comparison of annual cumulative footprints with their corresponding areas and SLB (δ, in %) for all the 12 sites. The SLBs higher than 5% are indicated in bold.

Tower ID[a]	Cumu_fp[b] (%)	Footprint size		SLB for A_r[d] = 90% footprint (scenario A)		SLB for A_r = circular area centred at individual towers with radii of					
		Area (km^2)	Radius[c] (km)			1 km (scenario B)		2 km (scenario C)		3 km (scenario D)	
				NDVI	EVI	NDVI	EVI	NDVI	EVI	NDVI	EVI
AB-GRS	80	1.456	0.681	1.032	0.130	−1.565	0.314	0.855	0.134	0.801	0.228
	90	1.937	0.785	0.787	0.097	−1.803	0.281	0.610	0.101	0.557	0.195
	99	2.759	0.937	1.023	0.059	−1.573	0.242	0.846	0.062	0.793	0.156
AB-WPL	80	1.032	0.573	0.656	−0.087	0.675	−0.185	−2.134	−0.021	−4.931	0.350
	90	1.369	0.660	0.485	−0.049	0.504	−0.147	−2.300	0.016	**−5.092**	0.388
	99	1.956	0.789	0.403	−0.032	0.422	−0.130	−2.380	0.034	**−5.170**	0.405
BC-DF49	80	2.801	0.944	−0.047	0.026	−0.392	0.013	−0.014	0.092	1.779	−0.013
	90	3.703	1.086	−0.007	0.016	−0.352	0.003	0.026	0.082	1.820	−0.022
	99	5.256	1.293	−0.091	0.015	−0.436	0.002	−0.058	0.082	1.734	−0.023
MB-NOBS	80	3.088	0.991	−1.972	1.464	−0.095	0.050	**−5.288**	4.209	**−6.353**	5.393
	90	4.082	1.140	−1.401	1.030	0.487	−0.379	−4.736	3.762	**−5.808**	4.941
	99	5.777	1.356	−0.705	0.511	1.196	−0.890	−4.064	3.230	−5.143	4.403
NB-OBF	80	1.928	0.783	**5.837**	−1.244	**6.812**	−0.857	**9.237**	**−5.171**	4.772	−2.532
	90	2.548	0.901	3.934	−0.764	4.891	−0.375	**7.273**	−4.710	2.888	−2.059
	99	3.605	1.071	1.814	0.149	2.752	0.542	**5.085**	−3.833	0.789	−1.157
ON-EPL	80	0.880	0.529	0.865	−1.898	3.560	**−5.728**	**12.225**	**−14.670**	**9.305**	**−12.681**
	90	1.142	0.603	0.528	−1.360	3.214	**−5.212**	**11.850**	**−14.202**	**8.940**	**−12.203**
	99	1.532	0.698	0.214	−0.868	2.892	−4.739	**11.501**	**−13.774**	**8.600**	**−11.765**
ON-OMW	80	2.900	0.961	0.507	−0.418	−0.877	2.560	4.752	**−8.681**	**5.138**	**−9.806**
	90	3.823	1.103	0.236	−0.035	−1.144	2.954	4.469	**−8.331**	4.854	**−9.460**
	99	5.393	1.310	−0.368	0.744	−1.740	3.756	3.839	**−7.616**	4.221	**−8.754**
ON-WPP39	80	2.620	0.913	−0.053	0.058	−0.132	−0.011	0.262	0.108	0.794	0.060
	90	3.481	1.053	−0.187	0.041	−0.266	−0.029	0.128	0.091	0.659	0.043
	99	4.948	1.255	−0.241	0.026	−0.321	−0.044	0.073	0.075	0.604	0.028
QC-EOBS	80	2.998	0.977	0.599	−0.090	−0.391	0.048	2.966	−0.456	1.050	−0.341
	90	3.959	1.123	0.273	−0.025	−0.714	0.114	2.633	−0.390	0.723	−0.275
	99	5.597	1.335	−0.160	0.039	−1.142	0.177	2.189	−0.327	0.288	−0.212
SK-OA	80	3.281	1.022	0.804	−1.110	−0.464	1.003	2.559	−2.917	**7.248**	**−6.696**
	90	4.347	1.176	0.563	−0.768	−0.702	1.353	2.313	−2.581	**6.991**	**−6.373**
	99	6.177	1.402	0.249	−0.371	−1.012	1.758	1.994	−2.192	**6.657**	**−5.999**
SK-OJP	80	3.596	1.070	−2.223	0.070	−0.480	0.005	**−6.228**	0.255	−4.965	0.199
	90	4.758	1.231	−1.449	0.048	0.308	−0.017	**−5.486**	0.233	−4.213	0.177
	99	6.757	1.467	−0.539	0.017	1.234	−0.048	−4.613	0.202	−3.328	0.146
SK-SOBS	80	3.812	1.101	−0.010	0.458	0.184	0.013	0.301	1.015	0.856	1.521
	90	5.043	1.267	−0.139	0.330	0.055	−0.115	0.172	0.886	0.726	1.392
	99	7.140	1.508	0.109	−0.043	0.302	−0.486	0.420	0.511	0.975	1.015

[a] See Table 1 for description of abbreviation of site name.
[b] Cumu_fp is annual cumulative footprint climatology percentage.
[c] The corresponding mean "radius" (r) is calculated by assuming the footprint is circular centred at the individual towers as $r_{\Pi} = \sqrt{A_{\Pi}/\pi}$, where A_{Π} is the footprint area for a given Π cumulative percentage (i.e. 80%, 90%, 99% in this table).
[d] A_r is the reference land surface area of interest, which is used in SLB calculation with Eq. (10).

annual and monthly SLBs were computed using NDVI and EVI as flux surrogates (Eqs. (8)–(10)).

In scenario A, the reference area of the ecosystem of interest (A_r) is assumed to be 90% of the annual footprint climatology area (A_{90}) for a specific sites. The annual SLBs for most of the FCRN sites were less than 5% using both NDVI and EVI as flux surrogates (Table 4). Exceptions included the NB-OBF site, where SLB δ = 5.8% (using NDVI as a flux surrogate) for the 80% footprint climatology which is likely due to the influence of a lake southwest of the tower and which is partly located within 90% of the annual footprint climatology area (Fig. 2). Fig. 6 shows variations of annual SLB using NDVI and EVI as flux surrogates with increasing cumulative footprint climatology percentages from 1% to 99% and with corresponding footprint climatology areas. For the 12 sites, the values of $|\delta|$ using NDVI and EVI as flux surrogates decreased with increasing footprint climatology size (or cumulative footprint percentage Π). The values of $|\delta|$ were considerable when the cumulative annual footprint climatology was less than 40% but were less than 5% using NDVI and 3% using EVI as a flux surrogate when Π > 80% (Fig. 6).

Using NDVI as a flux surrogate (Fig. 6a and c), sites NB-OBF and SK-OJP were found to have large $|\delta|$ values. For the 80% footprint climatology, the NB-OBF site overestimated the expected spatially aggregated flux over the ecosystem of interest (here $A_r = A_{90}$) by 5–10%, whereas the SK-OJP site underestimated the spatially aggregated flux by 5–15%. Using EVI as a flux surrogate (Fig. 6b and d), comparatively large absolute values of SLB ($|\delta|$ > 3%) were found at the following sites: ON-EPL, SK-OA, SK-SOBS and NB-OBF. The patterns of variations in δ with changes in the size of annual footprint climatology among the 12 sites were more diverse using EVI (Figs. 6b and d) as a flux surrogate than using NDVI (Figs. 6a and c). For instance, at ON-OMW the SLB for EVI varied within ±1.5% for a footprint of less than 40% (corresponding footprint area of ~1.0 km^2), followed by a gradual increase to 2.0% at the 55% footprint (corresponding footprint area of 1.8 km^2), then decreased to ~0% at the 65% footprint (corresponding footprint area of 2.1 km^2). This low values (<±1.0%) was maintained for greater footprint sizes. The SLB of the NB-OBF tower decreased with increasing footprint climatology size from 20% of Π (corresponding footprint area of 1.2 km^2) reaching about −2.5% at ~65% footprint climatology, followed by a gradual increase from −2.5% to approaching 0% at 99% annual footprint climatology. The differences in estimated δ using NDVI and EVI as surrogates further would likely suggest that the tower location biases are dependent on the land surface flux, which is consistent with the findings by Chen et al. (2009a).

Please cite this article in press as: Chen, B., et al., Assessing eddy-covariance flux tower location bias across the Fluxnet-Canada Research Network based on remote sensing and footprint modelling. Agric. Forest Meteorol. (2010), doi:10.1016/j.agrformet.2010.09.005

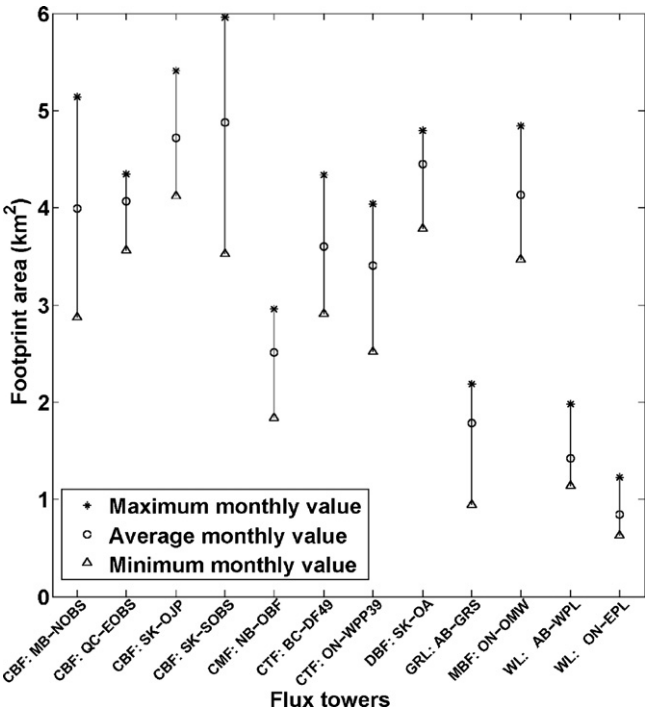

Fig. 5. Seasonal variations in the size of 90% footprint climatology for the 12 FCRN sites, presented by the maximum and minimum of monthly footprint climatology sizes. For description of abbreviation of vegetation type and site name, see Table 1.

In scenario B, A_r is assumed to be a circular area of 1-km radius centred at the individual towers. As shown in Table 4 and Fig. 7, the magnitudes and patterns of variations in annual SLB for NDVI and EVI with increasing cumulative footprint climatology percentages for the12 FCRN sites were similar to that in scenario A. The differences between scenarios A and B for most sites were: (i) the magnitudes of SLB for scenario B were about 10% higher than that for scenario A; and (ii) the values of $|\delta|$ monotonically decreased with increasing footprint size in scenario A, whereas in scenario B the $|\delta|$ starts to increased with increasing footprint size from the point when the footprint area reached a circular area of 1-km radius (i.e. 3.14 km^2, see Fig. 7c). Actually, the differences in SLB between scenarios A and B are inherently controlled by the differences in the land surface heterogeneity between A_{90} and the circular area of 1-km radius for an individual site. The SLB value of EVI for the SK-OA site in scenario A, for instance, was significantly larger than that in scenario B (Figs. 6c, d and 7c, d) because there is an area of shrub land north-west of the tower (within A_{90} but outside of the 1-km-radius circular area) that is quite heterogeneous (see Fig. 2, panel SK-OA).

In scenarios C and D (r = 2 km and 3 km, respectively), the magnitudes of $|\delta|$ were similar but generally larger than that in scenario B (Table 4). The variation in the patterns of SLB versus the footprint climatology area for most sites in scenarios C and D was similar to that in scenario B (not shown). The $|\delta|$ values using NDVI and EVI as flux surrogates for the ON-EPL wetland site approach 10% or greater. For the ON-OMW site (mixed wood boreal forest), the flux tower underestimated EVI by 7.5–10%, while overestimated NDVI by 4–5% (Table 4). For coniferous temperate forest sites (BC-DF49 and ON-WPP39), coniferous boreal forest sites (QC-EOBS and SK-SOBS) and the grassland site (AB-GRS), the differences between the tower perceived fluxes and the expected aggregates of land surface exchanges over different A_r were within 2% of the land surface source strength (Table 4). This holded for both using NDVI and EVI as flux surrogates and for all scenarios.

Fig. 8 shows the variations of annual SLB for the 90% footprint climatology using NDVI and EVI as flux surrogates with the corresponding reference circular areas of interest in Eq. (10) centred at the individual towers from radii (r) of 0.1–3 km. Diverse relationships existed between SLB and the size of A_r across the 12 sites, with SLB varying from −6 to 13% using NDVI and −14 to 5% using EVI as a flux surrogate. Using NDVI as a flux surrogate, Fig. 8a indicates that: (i) the coniferous temperate forest sites (BC-DF49 and ON-WPP39), coniferous boreal forest sites (QC-EOBS and SK-SOBS) and grassland site (AB-GRS) had low values of SLB ($|\delta| < 4\%$) throughout the range of A_r from approximately 0.3 to ∼10 km^2; the SLB of SK-OJP site decreased from 10.4% at r = 0.1 km to −5.8% at r = 1.9 km; and (iii) the SLBs for the coniferous maritime forest site (NB-OBF) and one wetland site (ON-EPL) rapidly increased from negative values to large positive values (>10%), followed by a gradual reduction to 2% and 9% at r = 3 km, respectively. As shown in Fig. 8b, six sites had very small variations in SLBs using EVI from r = 0.1 km throughout r = 3 km; these were the two coniferous temperate forest (CTF) sites (BC-DF49 and ON-WPP39), the grassland site (AB-GRS), one wetland site (AB-WPL) and two coniferous boreal forest (CBF) sites (MB-NOBS and QC-EOBS). The remaining sites had larger variations of SLB using EVI as a flux surrogate with increasing A_r, such as the ON-EPL wetland site, which varied from ∼4% to −14%. Overall for all sites, SLB values were low (<±5%) for both using NDVI and EVI as flux surrogates when $A_r \approx 1-3$ km^2 (i.e. $r \approx 0.5$–1 km).

Fig. 9 shows the seasonal variations in SLB using NDVI and EVI as flux surrogates with the 90% annual footprint climatology in scenarios A (A_r = 90% of annual footprint climatology area) and B (A_r = a circular area with 1-km radius centred at the individual towers). The seasonal differences in monthly SLB using NDVI as a surrogate were about 1–4% for most sites for both scenarios A and B (Fig. 9a), indicating small to moderate seasonal variations. Monthly SLB values at 6 of the sites were found to be identical. These towers we are the grassland site (AB-GRS), one wetland (AB-WPL), the two coniferous temperate forest sites (BC-DF49 and ON-WPP39) and two coniferous boreal forest sites (MB-NOBS and QC-EOBS). These six sites had very slight variations in SLB of EVI with A_r (Fig. 8b). Large seasonal variations in SLB for both NDVI and EVI were found at the following sites (Fig. 9): the coniferous maritime forest site (NB-OBF), the mixed wood boreal forest site (ON-OMW) and one coniferous boreal forest site (MB-NOBS). It is important to note that at the QC-EOBS site, the seasonal variations in SLB were large for NDVI but small for EVI. This likely suggests that the seasonal variation of SLB could be surface-flux dependent. We conducted regression analysis of the seasonal difference and seasonal standard deviation and mean of monthly SLB against the seasonal difference and seasonal standard deviation and mean of monthly footprint climatology size for all the sites. No significant relationship between SLB and footprint climatology PDF was found. This may indicate that neither seasonal variations in footprint climatology nor the different land surface flux components (e.g. using NDVI or EVI as flux surrogates) alone can explain the seasonal variations of SLB.

5. Discussion

The potential representativeness in EC flux measurements arising from the EC sensor's views over heterogeneous natural vegetation from different wind sectors, as mathematically defined as in Eqs. (8)–(10), were quantitatively assessed for FCRN tower sites. Our results (Figs. 6 and 7) demonstrate that the SLB absolute values ($|\delta|$) of flux measurements decreased with increasing size of the footprint climatology across a range of scenarios ($A_r = A_{90}$ or A_r = circular areas centred at the individual towers with r = 1 km, 2 km, 3 km). This is consistent with the results of Schmid and Lloyd (1999) for a Tiger bush site with large heterogeneities in the Sahel

Please cite this article in press as: Chen, B., et al., Assessing eddy-covariance flux tower location bias across the Fluxnet-Canada Research Network based on remote sensing and footprint modelling. Agric. Forest Meteorol. (2010), doi:10.1016/j.agrformet.2010.09.005

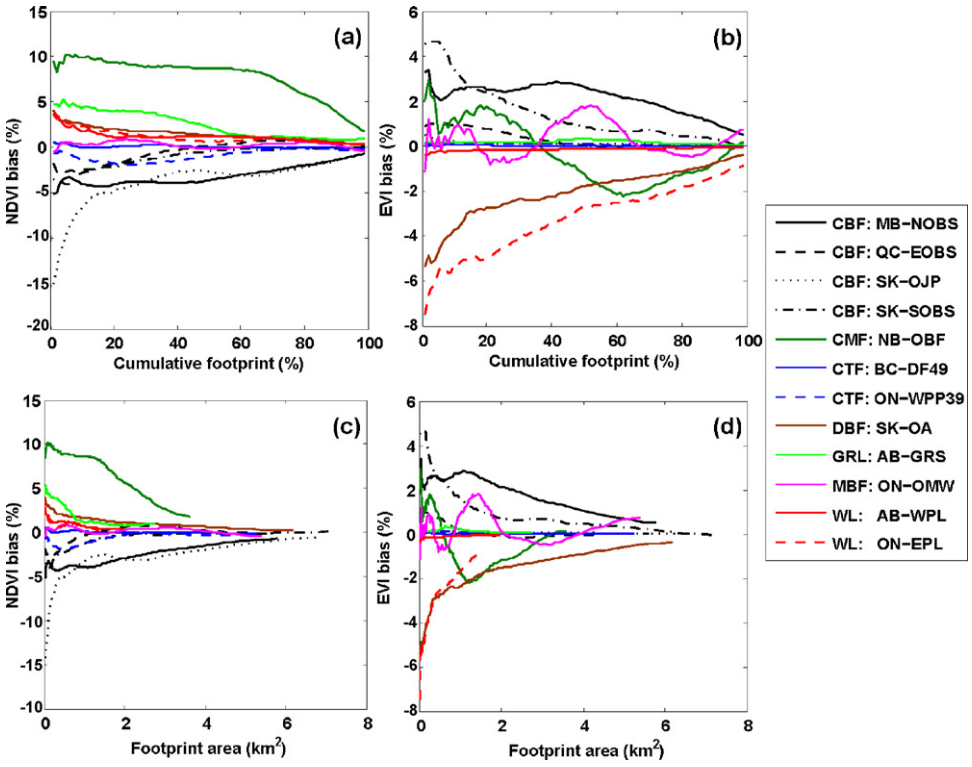

Fig. 6. Variations of annual sensor location biases using NDVI (a, c) and EVI (b, d) as flux surrogates with corresponding varying cumulative footprint climatology percentages (a, b) and footprint climatology areas (c, d) for the 12 FCRN sites. The reference area of interest in Eq. (10) was assumed to be 90% of annual footprint climatology (A_{90}) for individual sites, where A_{90} is the footprint area for 90% cumulative footprint percentage. For description of abbreviation of vegetation type and site name, see Table 1.

region of Niger. Figs. 6 and 7 indicate the SLB smoothly decreased with increasing footprint size if the heterogeneous land surface flux is arbitrari distributed across A_r. However, if clear surface discontinuities exist within A_r (such as water bodies) the monotonically decreasing $|\delta|$ curve is re-shaped (i.e. in the cases NB-OBF and ON-OMW) (Figs. 6 and 7). The relationship between $|\delta|$ and footprint size implies that the EC measured flux would be much less representative (higher bias) in unstable conditions than in stable

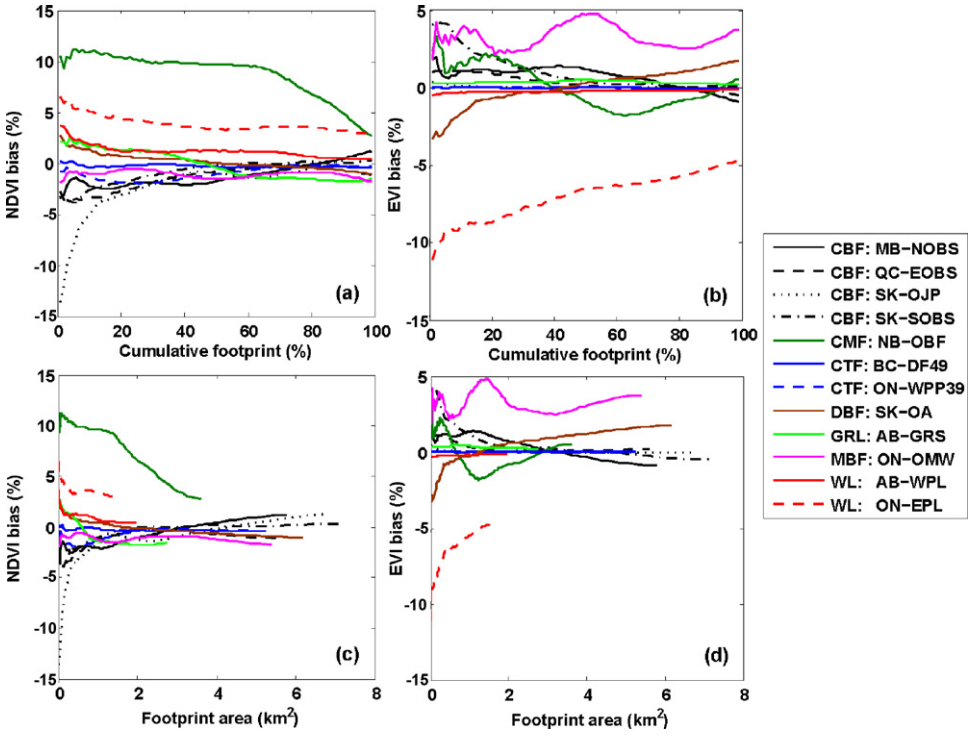

Fig. 7. Variations of annual sensor location biases using NDVI (a, c) and EVI (b, d) as flux surrogates with corresponding varying cumulative footprint climatology percentages (a, b) and footprint climatology areas (c, d) for the 12 FCRN sites. The reference area of interest in Eq. (10) is assumed to be a circular area with 1-km radius centred at the individual towers. For description of abbreviation of vegetation type and site name, see Table 1.

Please cite this article in press as: Chen, B., et al., Assessing eddy-covariance flux tower location bias across the Fluxnet-Canada Research Network based on remote sensing and footprint modelling. Agric. Forest Meteorol. (2010), doi:10.1016/j.agrformet.2010.09.005

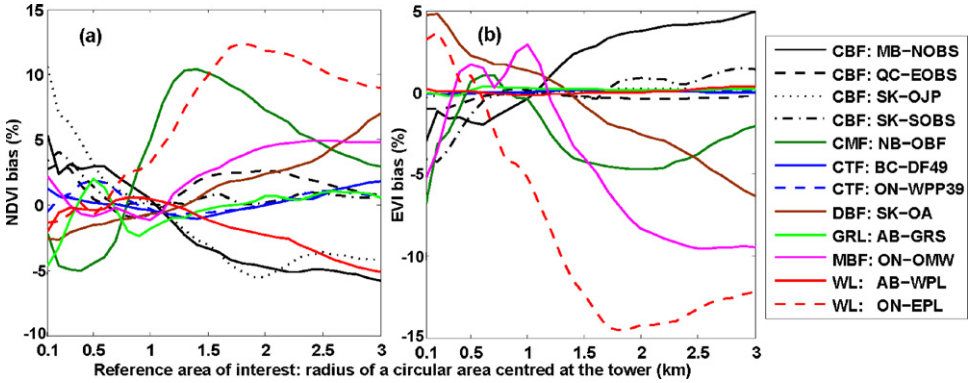

Fig. 8. Variations of annual sensor location biases using NDVI (a) and EVI (b) as flux surrogates for the 12 FCRN sites with corresponding varying reference circular areas of interest in Eq. (10) centred at the individual towers from radii of 0.1–3 km, while the cumulative footprint percentage in Eq. (9) was fixed to be 90%. For description of abbreviation of vegetation type and site name, see Table 1.

conditions because the footprint size is much smaller as atmospheric instability increases (Schmid and Lloyd, 1999; Chen et al., 2009a). Moreover, this relationship also tells us that the selection of the sensor mounting height should consider the land surface vegetation characteristics because the footprint size generally increases with the sensor height (Schmid, 1994, 1997; Schmid and Lloyd, 1999). Increasing the sensor height is a common activity for long-term monitoring of sites when the vegetation within the footprint area grows, however as the footprint size changes with sensor height this will also alter the sensor bias.

The mean value of $|\delta|$ throughout 1–99% of Π (i.e. $|\bar{\delta}|$) is a measure of the averaged land surface heterogeneity intensity within A_r. For scenario B (A_r = a circular area centred at the individual towers with r = 1 km), as indicated in Fig. 7, the two sites with the highest and second highest heterogeneity intensity were NB-OBF and ON-EPL and the most homogenous sites for NDVI were the two CTF sites. The *sill* (C) is a measure of total population variance, or absolute amount of heterogeneity in semivariogram analysis. The averaged SLB ($|\bar{\delta}|$) was not significantly correlated with the *sill* ($R^2 = 0.61$, $p = 0.12$) (Chen et al., submitted for publication). The semivariogram analysis is solely based on remote sensing data to detect the useful anisotropy information whereas $|\bar{\delta}|$ also strongly depends on the site climatology of wind direction and atmospheric stability.

On the basis of the combination of results using both NDVI and EVI as flux surrogates (indicated in Fig. 8), we conclude that eight FCRN towers would represent most of the ecosystem surrounding the individual towers from 0.3 km^2 up to an area of 10 km^2 with a satisfactorily low bias ($|\delta| < 5\%$). These towers were: AB-GRS, AB-WPL, BC-DF49, ON-OMW, ON-WPP39, WC-EOBS, SK-OA, and SK-SOBS. The remaining towers, however, represent a particular circular area. Using the radius of the circular area centred at the tower as a measure, the surrounding ecosystem would be well-represented (i.e. with a target of $|\delta| < 5\%$) by the EC tower measurements as: for the ON-EPL site, $r < \sim 0.75$ km; for MB-NOBS, $r < \sim 1.5$ km; for NB-OBF, $r = \sim 0.5$–1 km; and for SK-OJP site, $r = 0.5$–1.25 km. This information detected by SLB analysis is important and useful for assessing/explanation of the long-term EC measurements, especially for up-scaling of the EC fluxes to landscape or regional scales.

Biases in footprint climatology estimates will lead to uncertainty in tower location bias assessment. The SAFE footprint model used in this study applies to most conditions of atmo-

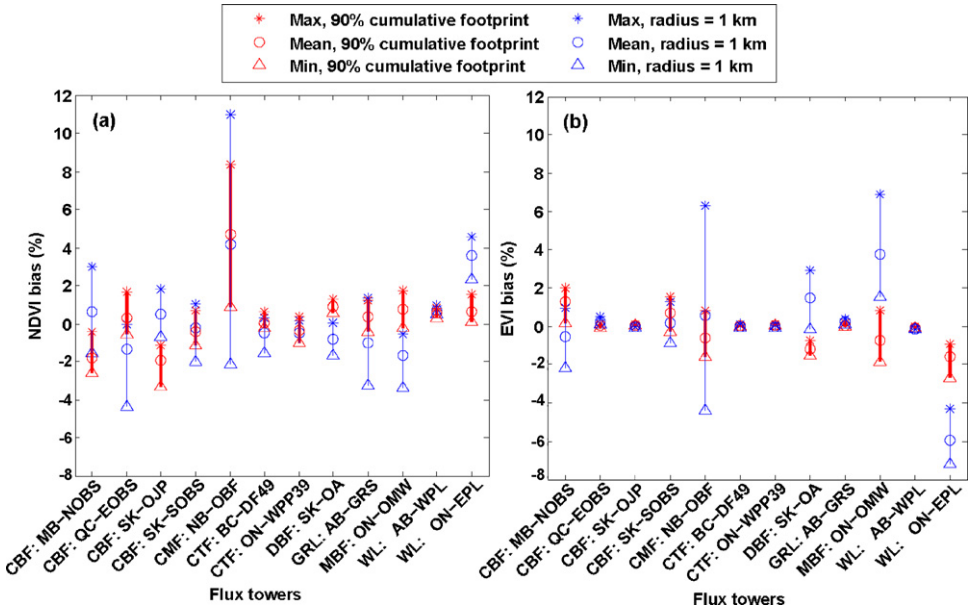

Fig. 9. Seasonal variations in sensor location biases (SLB) using NDVI and EVI as flux surrogates with 90% footprint climatology for the 12 FCRN sites, presented by the maximum and minimum of monthly SLB. The reference areas of interest in Eq. (10) were 90% of annual footprint climatology area and a circular area with 1-km radius centred at the individual towers, respectively. For description of abbreviation of vegetation type and site name, see Table 1.

Please cite this article in press as: Chen, B., et al., Assessing eddy-covariance flux tower location bias across the Fluxnet-Canada Research Network based on remote sensing and footprint modelling. Agric. Forest Meteorol. (2010), doi:10.1016/j.agrformet.2010.09.005

spheric stability using a stationary gradient diffusion formulation with height-independent crosswind dispersion. The assumption of independence of vertical and crosswind dispersion allows the reduction of the continuity equation to a two-dimensional advection-diffusion equation. Model comparison results showed that in unstable or neutral conditions when the mean plume height was high, the analytical models tend to be biased with a long tail, shorter peak value and the peak location farther from the receptor. To avoid the model biases resulting from this limitation of the analytical model, the source area Ω_{Π} is considered to be all of the grids (cells) that have $f(x,y,z_m)$ larger than the cut-off point, where a given cumulative fraction Π (e.g. 95%, or 97%) is achieved (Chen et al., 2009a). Hence, the biases in footprint climatology estimation using SAFE are approximately within 5% of other models.

Chen et al. (2009a) reported that the weighted footprint climatology significantly varied with the different flux components. In order to confirm their findings and compare the differences in SLB estimation between using different indices, we used both NDVI and EVI as the surrogates of land surface source strength in the current study. In this sense, the SLB assessment using NDVI and EVI as flux surrogates is only a first-order estimate. In addition, given large seasonal variations of carbon and water fluxes and the satellite image analysis with a limited dataset (one image for the whole year in this study), the uncertainty and bias in the sensor-bias estimation are worth considering. LANDSAT imagery at a 30-m spatial resolution is well suited for characterizing landscape-level forest structure and is ideal for SLB analysis. Its 16-day revisit-cycle, is however, generally lengthened by frequent cloud contamination and other poor atmospheric conditions (Ju and Roy, 2007). At the FCRN sites, for instance, there are a very limited number of scenes available in, or close to, 2006, which limits the study of the seasonality of vegetation dynamics. As a result we only selected one scene for each site during the growing season (Table 3). We deemed this appropriate as the analysis was focused on the annual SLB and the relative variability of NDVI and EVI within the selected domain, rather than their absolute values. Following Kim et al. (2006), the use of the single LANDSAT derived NDVI or EVI to estimate SLB over an extended period (i.e. monthly and annual) relies on the assumption that seasonal variations of vegetation indices affect all areas within the 6 km × 6 km domain proportionally, with a similar phenological development for individual sites. Moreover, due to the limitation of LANDSAT data availability, the imagery data used in this study acquired across a range of years (1999–2006; Table 3), also impacts the comparison of SLB between sites. As a result, we acknowledge our results are based on the assumption that the relative variability observed in the vegetation indices does not change across years within the footprint area. Under this assumption we believe the SLB analysis using vegetation indices in this study is useful. Future work is needed to estimate more accurately the δ of carbon flux and water flux components using flux field data, which can be derived from a combination of remote sensing and process-based ecosystem modelling approaches.

6. Summary and conclusions

We evaluated the sensor location bias of 12 Fluxnet Canada Research Network (FCRN)/Canadian Carbon Program (CCP) flux sites that included grassland, wetland and temporal and boreal forests across an east-west continental gradient using a footprint model and moderate spatial resolution remote sensed data. Monthly and annual footprint climatologies were estimated and the size of the 90% cumulative footprint climatology varied from 1.1 km^2 (at ON-EPL) to 5.0 km^2 (at SK-SOBS) across the sites. The footprint and footprint climatology PDFs were overlaid on the NDVI and EVI maps to estimate the sensor location bias (SLB). Our results show that (i) the sizes of annual footprint climatologies increased exponentially with increasing cumulative footprint percentages and varied in increasing rates among sites; (ii) the estimated SLB using both NDVI and EVI as flux surrogates with respect of the area of interest (A_r) at the 90% annual footprint climatology (scenario A) and a circular area with radius of 1 km centred at the individual tower (scenario B) was less than 5% for most FCRN sites. Several sites had larger biases, for example, the SLBs using NDVI as a flux surrogate at the NB-OBF site were about 5.8% and 6.8% at a 90% footprint area for scenarios A and B, respectively; (iii) the SLB decreased with increasing size of footprint climatologies for all sites and scenarios, suggesting that the EC measured flux in strongly unstable conditions would be much less representative (higher bias) than in neutral/stable conditions; (iv) out of 12, eight FCRN towers represented most of the ecosystem surrounding the individual towers from 0.3 km^2 up to an area of 10 km^2 with a satisfactorily low bias ($|\delta| < 5\%$), whereas the four remaining towers represented areas (i.e. with a target of $|\delta| < 5\%$) ranging from only ~0.75 to ~4 km^2. This information detected by SLB analysis is useful for assessing long-term EC measurements, especially for up-scaling of the EC fluxes to landscape or regional scales; and (v) the seasonal differences in monthly SLB using NDVI as a flux surrogate were about 1–4% for most sites for both scenarios A and B.

Acknowledgements

This research was financially supported by an Alexander Graham Bell Canada Scholarship (CGS) funded by the Natural Sciences and Engineering Research Council of Canada (NSERC), by "One hundred talents" program funded by Chinese Academy of Sciences, by the National Science Foundation of China (Grant No. 41071059), by the National Key Technology R&D Program of China (Grant No. 2008BAK50B06-02), by the National Basic Research Program of China (Grant Nos. 2010CB950900 and 2010CB950704), and by Fluxnet-Canada Research Network (FCRN)/Canadian Carbon Program (CCP) funds provided by NSERC, the Canadian Foundation for Climate and Atmospheric Sciences (CFCAS) and BIOCAP Canada. Contribution of researcher involved in data collected and in-kind support from many government and private agencies for each study site are also acknowledged. We gratefully acknowledge the constructive comments of the associate editor Dr. M. Susan Moran and two anonymous reviewers on an earlier version of this manuscript.

References

Admiral, S.W., Lafleur, P.M., 2007. Modelling of latent heat partitioning at a bog peatland. Agricultural and Forest Meteorology 144, 213–229.
Amiro, B.D., 1998. Footprint climatologies for evapotranspiration in a boreal catchment. Agricultural and Forest Meteorology 90, 195–201.
Arain, M.A., Restrepo-Coupe, N., 2005. Net ecosystem production in a temperate pine plantation in southeastern Canada. Agricultural and Forest Meteorology 128, 223–241.
Baldocchi, D.D., 2003. Assessing the eddy covariance technique for evaluating carbon dioxide exchange rates of ecosystems: past, present and future. Global Change Biology 9, 479–492.
Baldocchi, D.D., 2008. Breathing of the terrestrial biosphere: lessons learned from a global network of carbon dioxide flux measurement systems. Australian Journal of Botany 56, 1–26.
Barr, A.G., Morgenstern, K., Black, T.A., McCaughey, J.H., Nesic, Z., 2006. Surface energy balance closure by the eddy-covariance method above three boreal forest stands and implications for the measurement of the CO_2 flux. Agricultural and Forest Meteorology 140, 322–337.
Bergheime, J., Wilske, B., Maseyk, K., Karnieli, A., Zaady, E., Yakir, D., Kesselmeier, J., 2006. Relationships between Normalized Difference Vegetation Index (NDVI) and carbon fluxes of biologic soil crusts assessed by ground measurements. Journal of Arid Environments 64, 651–669.
Chasmer, L., Kljun, N., Barr, A., Black, A., Hopkinson, C., McCaughey, H., Treitz, P., 2008. Influences of vegetation structure and elevation on CO_2 uptake in a mature jack pine forest in Saskatchewan, Canada. Canadian Journal of Forest Research 38, 2746–2761.
Chen, B., Black, A., Coops, N.C., Hilker, T., Trofymow, T., Nesic, Z., Morgenstern, K., 2009a. Assessing tower flux footprint climatology and scaling between remotely sensed and eddy covariance measurements. Boundary-Layer Meteorology 130, 137–167.

Please cite this article in press as: Chen, B., et al., Assessing eddy-covariance flux tower location bias across the Fluxnet-Canada Research Network based on remote sensing and footprint modelling. Agric. Forest Meteorol. (2010), doi:10.1016/j.agrformet.2010.09.005

Chen, B., Black, A., Coops, N.C., Jassal, R., Nesic, Z., 2009b. Seasonal controls on interannual variability in carbon dioxide exchange of a Pacific Northwest Douglas-fir forest, 1997–2006. Global Change Biology 15, 1962–1981.

Chen, B., Chen, J.M., Mo, G., Yuen, C.-W., Margolis, H., Higuchi, K., Chan, D., 2007. Modeling and scaling coupled energy, water, and carbon fluxes based on remote sensing: an application to Canada's landmass. Journal of Hydrometeorology 8, 123–143.

Chen, B., Chen, J.M., Mo, G., Black, T.A., Worthy, D.E.J., 2008. Comparison of regional carbon flux estimates from CO_2 concentration measurements and remote sensing based footprint integration. Global Biogeochemical Cycles 22, GB2012, doi:10.1029/2007GB003024.

Chen, B., Coops, N.C., Margolis, H.A., Barr, A.G., Black, T.A., Amiro, B.D., Arain, M.A., Bourque, C. P.-A., Flanagan, L.B., Lafleur, P.M., McCaughey, J. H., Wofsy, S.C., submitted for publication. Characterizing the spatial variation of eddy-covariance flux tower's footprint area across the Fluxnet-Canada Research Network. Agricultural and Forest Meteorology (in review).

Dunn, A., Barforsw, C.C., Wofsy, S., Goulden, M.L., Daube, B.C., 2007. A long-term record of carbon exchange in a boreal black spruce forest: means, responses to interannual variability and decadal trends. Global Change Biology 12, 1–14.

Field, C.B., Randerson, J.T., Malmstrom, C.M., 1995. Global net primary production-combining ecology and remote sensing. Remote Sensing of Environment 51, 74–88.

Finn, D., Lamb, B., Leclerc, M.Y., Horst, T.W., 1996. Experimental evaluation of analytical and Lagrangian surface-layer flux footprint models. Boundary-Layer Meteorology 80, 283–308.

Finnigan, J.J., Clement, R., Malhi, Y., Leuning, R., Cleugh, H.A., 2003. A re-evaluation of long-term flux measurement techniques. Part I: averaging and coordinate rotation. Boundary-Layer Meteorology 107, 1–48.

Flanagan, L.B., 2009. Phenology of plant production in the northwestern great plains: relationships with carbon isotope discrimination, net ecosystem productivity and ecosystem respiration. In: Noormets, A. (Ed.), Phenology of Ecosystem Processes. Springer Science, Business Media, New York, pp. 169–185.

Flanagan, L.B., Johnson, B.G., 2005. Interacting effects of temperature, soil moisture and plant biomass production on ecosystem respiration in a northern temperate grassland. Agricultural and Forest Meteorology 130, 237–253.

Flanagan, L.B., Wever, L.A., Carlson, P.J., 2002. Seasonal and interannual variation in carbon dioxide exchange and carbon balance in a northern temperate grassland. Global Change Biology 8, 599–615.

Foken, T., Wichura, B., 1996. Tools for quality assessment of surface-based flux measurements. Agricultural and Forest Meteorology 78, 83–105.

Gockede, M., Rebmann, C., Foken, T., 2004. A combination of quality assessment tools for eddy covariance measurements with footprint modelling for the characterisation of complex sites. Agricultural and Forest Meteorology 127, 175–188.

Goulden, M.L., Munger, J.W., Fan, S.M., Daube, B.C., Wofsy, S.C., 1996. Measurements of carbon sequestration by long-term eddy covariance: methods and a critical evaluation of accuracy. Global Change Biology 2, 169–182.

Govind, A., Chen, J.M., Ju, W., 2009. Spatially explicit simulation of hydrologically controlled carbon and nitrogen cycles and associated feedback mechanisms in a boreal ecosystem. Journal of Geophysical Research 114, G02006, doi:10.1029/2008JG000728.

Gryning, S.E., Holtslag, A.A.M., Irvin, J.S., Sivertsen, D., 1987. Applied dispersion modeling based on meteorological scaling parameters. Atmospheric Environment 21, 79–89.

Hall, F., Sellers, P., Strebel, D., Kanemasu, E., Kelly, R., Blad, B., Markham, B., Wang, J., Huemmrich, F., 1991. Satellite remote sensing of surface energy and mass balance results: results from FIFE. Remote Sensing of Environment 35, 187–199.

Holifield, C.D., McElroy, S., Moran, M.S., Bryant, R., Miura, T., 2003. Temporal and spatial changes in grassland transpiration detected using Landsat TM and ETM+ imagery, Canadian. Journal of Remote Sensing 29, 259–270.

Horst, T.W., Weil, J.C., 1992. Footprint estimation for scalar flux measurements in the atmospheric surface layer. Boundary-Layer Meteorology 59, 279–296.

Horst, T.W., Weil, J.C., 1994. How far is far enough? the fetch requirements of micrometeorological measurement of surface fluxes. Journal of Atmospheric and Oceanic Technology 11, 1018–1025.

Huete, A.R., Liu, H.Q., Batchily, K., van Leeuwen, W., 1997. A comparison of vegetation indices over a global set of TM images for EOS-MODIS. Remote Sensing of Environment 59, 440–451.

Ju, J.C., Roy, D.P., 2007. The availability of cloud-free Landsat ETM+ data over the conterminous United States and globally. Remote Sensing of the Environment 112, 1196–1211.

Kim, J., Guo, Q., Baldocchi, D.D., Xu, L., Leclerc, M.Y., 2006. Upscaling CO_2 fluxes from tower to landscape: overlaying tower flux footprint calculations on high resolution (IKONOS) vegetation density images. Agricultural and Forest Meteorology 136, 132–146.

Kormann, R., Meixner, F.X., 2001. An analytic footprint model for neutral stratification. Boundary-Layer Meteorology 99, 207–224.

Leclerc, M.Y., Meskhidz, N., Finn, D., 2003. Comparison between measured tracer fluxes and footprint model predictions over a homogeneous canopy of intermediate roughness. Agricultural and Forest Meteorology 117, 145–158.

Leclerc, M.Y., Thurtell, G.W., 1990. Footprint predictions of scalar fluxes using a Markovian analysis. Boundary-Layer Meteorology 52, 247–258.

McCaughey, J.H., Pejam, M.R., Arain, M.A., Cameron, D.A., 2006. Carbon dioxide and energy fluxes from a boreal mixed wood forest ecosystem in Ontario, Canada. Agricultural and Forest Meteorology 140, 79–96.

Moran, M.S., Inoue, Y., Barnes, E.M., 1997. Opportunities and limitations for image-based remote sensing in precision crop management. Remote Sensing of Environment 61, 319–346.

Moran, M.S., Jackson, R.D., 1991. Assessing the spatial distribution of evapotranspiration using remotely sensed inputs. Journal of Environmental Quality 20, 725–737.

Moran, M.S., Kustas, W.P., Vidal, A., Stannard, D.I., Blanford, J.H., Nichols, W.D., 1994. Use of ground-based remotely sensed data for surface energy balance evaluation of a semiarid rangeland. Water Resources Research 30, 1339–1350.

Moran, M.S., Maas, S.J., Pinter Jr., P.J., 1995. Combining remote sensing and modeling for estimating surface evaporation and biomass production. Remote Sensing Reviews 12, 335–353.

Moran, M.S., Rahman, A.F., Washburne, J.C., Goodrich, D.C., Weltz, M.A., Kustas, W.P., 1996. Combining the Penman–Monteith equation with measurements of surface temperature and reflectance to estimate evaporation rates of semiarid grassland. Agricultural And Forest Meteorology 80, 87–109.

Nappo, C.J., Caneill, J.Y., Furman, R.W., Gifford, F.A., Kaimal, J.C., Kramer, M.L., Lockhart, T.J., Pendergast, M.M., Pielke, R.A., Randerson, D., Shreffler, J.H., Wyngaard, J.C., 1982. The workshop on the representativeness of meteorological observations, June 1981, Boulder, Colo. Bulletin of the American Meteorological Society 63, 761–764.

Nouvellon, Y., Moran, M.S., Lo Seen, D., Bryant, R., Rambal, S., Ni, W., Bégue, A., et al., 2001. Coupling a grassland ecosystem model with Landsat imagery for a 10-year simulation of carbon and water budgets. Remote Sensing of Environment 78, 131–149.

Pasquill, F., Smith, F.B., 1983. Atmospheric Diffusion, 3rd ed. Wiley, 437pp.

Peichl, M., Brodeur, J.J., Khomik, M., Arain, M.A., 2010. Biometric and eddy-covariance based estimates of carbon fluxes in an age-sequence of temperate pine forests. Agricultural and Forest Meteorology 150, 952–965.

Rebmann, C., Goekede, M., Foken, T., Aubinet, M., Aurela, M., Berbigier, P., Bernhofer, C., Buchmann, N., Carrara, A., Cescatti, A., Ceulemans, R., Clement, R., Elbers, J.A., Granier, A., Gr¨unwald, T., Guyon, D., Havrˇankovˇa, K., Heinesch, B., Knohl, A., Laurila, T., Longdoz, B., Marcolla, B., Markkanen, T., Miglietta, F., Moncrieff, J., Montagnani, L., Moors, E., Nardino, M., Ourcival, J.M., Rambal, S., Rannik, A., Rotenberg, E., Sedlak, P., Unterhuber, G., Vesala, T., Yakir, D., 2005. Quality analysis applied on eddy covariance measurements at complex forest sites using footprint modelling. Theoretical and Applied Climatology 80, 121–141.

Richardson, A.D., Hollinger, D.Y., Burba, G.G., Davis, K.J., Flanagan, L.B., Katul, G.G., Munger, J.W., Ricciuto, D.M., Stoy, P.C., Suyker, A.E., Verma, S.B., Wofsy, S.C., 2006. A multi-site analysis of random error in tower-based measurements of carbon and energy fluxes. Agricultural and Forest Meteorology 136, 1–18.

Running, S.W., Nemani, R.R., Heinsch, F.A., Zhao, M., Reeves, M., Jolly, M.A., 2004. Continuous satellite-derived measure of global terrestrial primary productivity: future science and applications. Bioscience 56, 547–560.

Schmid, H.P., 1994. Source areas for scalar and scalar fluxes. Boundary-Layer Meteorology 67, 293–318.

Schmid, H.P., 1997. Experimental design for flux measurements: matching scales of observations and fluxes. Agricultural and Forest Meteorology 87, 179–200.

Schmid, H.P., 2002. Footprint modeling for vegetation atmosphere exchange studies: a review and perspective. Agricultural and Forest Meteorology 113, 159–183.

Schmid, H.P., Lloyd, C.R., 1999. Spatial representativeness and the location bias of flux footprint over inhomogeneous areas. Agricultural and Forest Meteorology 93, 195–209.

Sellers, P.J., 1985. Canopy reflectance, photosynthesis and transpiration. International Journal of Remote Sensing 6, 1335–1372.

Soegaard, H., Jensen, N.O., Boegh, E., Hasager, C.B., Schelde, K., Thomsen, A., 2003. Carbon dioxide exchange over agricultural landscape using eddy correlation and footprint modelling. Agricultural and Forest Meteorology 114, 153–173.

Stoughton, T.E., Miller, D.R., Yang, X., Hendrey, G.M., 2000. Footprint climatology estimation of potential control ring contamination at the Duke Forest FACTS-1 experiment site. Agricultural and Forest Meteorology 100, 73–82.

Syed, K.H., Flanagan, L.B., Carlson, P.J., Glenn, A.J., Van Gaalen, K.E., 2006. Environmental control of net ecosystem CO_2 exchange and carbon balance in a treed, moderately rich fen in northern Alberta. Agricultural and Forest Meteorology 140, 97–114.

Tucker, C.J., 1979. Red and photographic infrared linear combinations for monitoring vegetation. Remote Sensing of Environment 8, 127–150.

Turner, D.P., Urbanski, S., Bremer, D., Wofsy, S.C., Meyers, T., Gower, S.T., Gregory, M., 2003. A cross-biome comparison of daily light use efficiency for gross primary production. Global Change Biology 9, 383–395.

van Ulden, A.P., 1978. Simple estimates for vertical diffusion from sources near the ground. Atmospheric Environment 12, 2125–2129.

Wilson, J.D., Swaters, G.E., 1991. The source area influencing a measurement in the planetary boundary layer: the footprint and the distribution of contact distance. Boundary-Layer Meteorology 55, 25–46.

Wu, J.D., Wang, D., Bauer, M.E., 2005. Image-based atmospheric correction of QuickBird imagery of Minnesota cropland. Remote Sensing of Environment 99, 315–325.

Xiao, X., Hollinger, D., Aber, J.D., Goltz, M., Davidson, E., Zhang, Q., Moore III, B., 2004. Satellite-based modeling of gross primary production in an evergreen needle leaf forest. Remote Sensing of Environment 89, 519–534.

Xing, Z., Bourque, C.P.-A., Meng, F., Zha, T., Cox, R.M., Swift, D.E., 2007. A simple net ecosystem productivity model for gap filling of tower-based fluxes: an extension of Landsberg's equation with modifications to the light interception term. Ecological modelling 206, 250–262.

Please cite this article in press as: Chen, B., et al., Assessing eddy-covariance flux tower location bias across the Fluxnet-Canada Research Network based on remote sensing and footprint modelling. Agric. Forest Meteorol. (2010), doi:10.1016/j.agrformet.2010.09.005